On the Interpretation of the Observed Linear Free Energy Relationship in Phosphate Hydrolysis: A Thorough Computational Study of Phosphate Diester Hydrolysis in Solution†

Edina Rosta, Shina C. L. Kamerlin,* and Arieh Warshel*

Department of Chemistry, University of Southern California, 3620 McClintock Avenue, Los Angeles, California 90089-1062

Received October 18, 2007; Revised Manuscript Received January 5, 2008

ABSTRACT: The hydrolysis of phosphate esters is crucially important to biological systems, being involved in, among other things, signaling, energy transduction, biosynthesis, and the regulation of protein function. Despite this, there are many questions that remain unanswered in this important field, particularly with regard to the preferred mechanism of hydrolysis of phosphate esters, which can proceed through any of multiple pathways that are either associative or dissociative in nature. Previous comparisons of calculated and observed linear free energy relationships (LFERs) for phosphate monoester dianions with different leaving groups showed that the TS character gradually changes from associative to dissociative with the increasing acidity of the leaving group, while reproducing the experimental LFER. Here, we have generated *ab initio* potential energy surfaces for the hydrolysis of phosphate diesters in solution, with a variety of leaving groups. Once again, the reaction changes from a compact concerted pathway to one that is more expansive in character when the acidity of the leaving group increases. When such systems are examined in solution, it is essential to take into consideration the contribution of solute to the overall activation entropy, which remains a major computational challenge. The popular method of calculating the entropy using a quasi-harmonic approximation appears to markedly overestimate the configurational entropy for systems with multiple occupied energy wells. We introduce an improved restraint release approach for evaluating configurational entropies and apply this approach to our systems. We demonstrate that when this factor is taken into account, it is possible to reproduce the experimental LFER for this system with reasonable accuracy.

Phosphate ester hydrolysis is a crucially important reaction in biological systems, being involved in, among other things, signal and energy transduction, biosynthesis, protein synthesis, and replication of the genetic material (*1–6*). Phosphoric acid can in principle be esterified at any or all of three positions, forming phosphate monoesters, diesters, or triesters, and the reaction mechanism will vary according to the system (*1*). Attack of hydroxide on the phosphorus atom will, however, generally proceed through one of three different pathways (*1, 7–13*) (Scheme 1).

Hydrolysis by hydroxide attack may proceed through one of two stepwise pathways: a dissociative S_N1-type ($D_N + A_N$) mechanism in which leaving group departure precedes nucleophilic attack and the reaction proceeds via a trivalent intermediate (Scheme 1, A) or an associative ($A_N + D_N$) mechanism in which the nucleophile attacks prior to leaving group departure and the reaction proceeds via a pentavalent intermediate (Scheme 1, B). There is, however, a third possibility that involves a concerted (A_ND_N) process, in which bond making and bond breaking occur in a single reaction step. As a result, in contrast to the stepwise pathways, this reaction passes through a single transition state structure without an intermediate (Scheme 1, C). When stepwise pathways are being discussed, it is comparatively easy to describe the mechanism as either associative or dissociative. However, the situation for concerted pathways is more complex. A concerted transition state may be either synchronous (with roughly equal amounts of bonding to both the leaving group and the nucleophile) or asynchronous. In addition, an asynchronous transition state can be either associative, with a larger degree of bond formation to the nucleophile than breaking of the bond to the leaving group, or dissociative, with more bond breaking than bond forma-

Scheme 1: Hypothetical Pathways for Phosphate Diester Hydrolysis

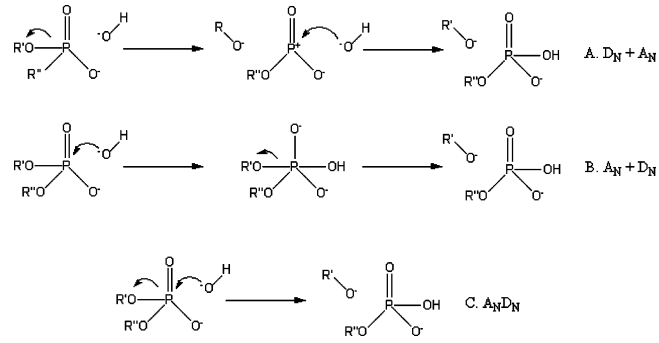

† This work was supported by NCI Grant 1 U19 CA105010-01 and NSF Grant MCB-0342276. All computational work was supported by the University of Southern California High Performance Computing and Communication Center.

* To whom correspondence should be addressed. E-mail: l.kamerlin@gmx.at or warshel@usc.edu. Telephone: (213) 740-4114. Fax: (213) 740-2701.

10.1021/bi702106m CCC: $40.75
Published on Web 02/29/2008

tion. In recent years, some authors have adapted to this issue by referring to concerted mechanisms as proceeding via "tight" or "loose" transition states (e.g., refs *14–19*).

Unfortunately, such a description can be deceptive, as it is rather vague and implies a cutoff between two mechanistic possibilities, which is the case with the stepwise pathways. However, it is very important to understand that this cutoff is actually not clear and that concerted transition states rather lie on a spectrum between more compact associative and more expansive dissociative transition states. As we shall demonstrate in this work, these differences can be quite subtle, and it is important to proceed with caution when describing such pathways.

Not surprisingly, considering the range of mechanistic possibilities, a wide variety of enzymes which catalyze phosphate ester hydrolysis exist. For instance, the GTP-hydrolase RAS is a phosphate monoesterase which catalyzes the hydrolysis of GTP to GDP (*20*). It is now widely agreed that the reaction is not catalyzed by a general base (*21–23*) and that the water proton is transferred to the γ-phosphate (which can thus be considered to be the effective base) (*22, 24–26*). The precise mechanism of the attack of the water molecule is still controversial (*21–23, 25–33*); nevertheless, a careful exploration of the free energy surface for the GTPase reaction of the RasGap system suggests that the preferred transition state for this reaction is associative (*10*). Furthermore, it was found that the customary assumption that the mechanism of the reference solution reaction is dissociative is very problematic (*10*). Another important example is presented by the DNA polymerases which are phosphate diesterases responsible for regulating a wide range of activities, including DNA repair, DNA recombination, and damage bypassing, all functions which are absolutely essential in maintaining the integrity of the genome (*34*). The exact mechanism of the catalytic reaction is also not clear in this case (see, for example, refs *35–41*), and more systematic studies are needed.

An interesting example of an enzyme that catalyzes phosphate ester hydrolysis is *Escherichia coli* alkaline phosphatase (AP). This is a metalloenzyme that catalyzes the hydrolysis of a broad range of not only phosphate monoester but also diester substrates, presumably to harvest phosphate for nucleic acids or various metabolites, providing rate enhancements of greater than 10^{17}-fold for phosphate monoesters and 10^{11}-fold for phosphate diesters (*14, 42, 43*). However, despite the common preference of AP for phosphate monoester hydrolysis, evolutionarily related homologues that preferentially catalyze phosphate diester hydrolysis exist, which suggests that the AP active site is able not only to recognize but also to distinguish between different transition states (*44–46*). Understanding the factors controlling the selectivity of AP is clearly of great importance. Such an understanding should be combined with a deeper understanding of phosphatases that exclusively catalyze phosphate mono- or diesters.

In view of the complexity of enzyme-catalyzed phosphate ester hydrolysis, it is essential to have a clear understanding of the corresponding solution reactions. This is not only important in obtaining a general understanding of the reaction mechanism but also crucial for the calibration and validation of theoretical models that are being used to probe enzymatic phosphate ester hydrolysis, which has been previously

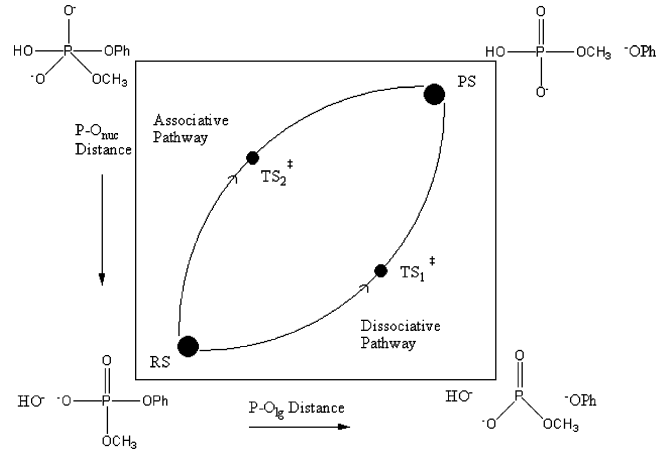

FIGURE 1: Free energy surface for phosphate diester hydrolysis.

demonstrated in studies of phosphate monoesters (*10*). Also, as discussed below, the interpretation of the available experimental information is far from obvious. The same situation most likely holds for phosphate diester hydrolysis, which is the focus of this study.

A well-known experimental method for studying reaction mechanisms involves the use of linear free energy relationships (LFERs)[1] (*47, 48*). This approach involves studying a series of homologous compounds with various pK_a values. Kinetic measurements are performed on this series, and the logarithm of the rate constant is correlated to the pK_a of the leaving group such that

$$\log(k) = \beta_{lg} pK_a + C \quad (1)$$

The Brønsted coefficient, β_{lg} (obtained from the gradient of the LFER), measures the leaving group dependence of the reaction series. A reaction proceeding through a dissociative mechanism would be expected to have a large negative value of β_{lg}, and conversely, a reaction proceeding through an associative mechanism would be less dependent on the nature of the leaving group and would proceed via a smaller value of β_{lg}. This approach is not, however, without a number of shortcomings. First, LFERs cannot distinguish between concerted (A_ND_N) and stepwise ($A_N + D_N$ or $D_N + A_N$) mechanisms. Second, several studies have shown that as LFERs are not based on direct molecular information, they need not have unique mechanistic interpretations, and associative and dissociative pathways can be equally viable for the same LFER (*10, 49, 50*).

The free energy surface for phosphate diester hydrolysis can be represented by a More O'Ferral Jencks (MFJ) plot (Figure 1) (*51, 52*), which defines the energy surface in terms of two reaction coordinates. In Figure 1, reactants are located at the bottom left and products at the top right corners of the plot. An associative ($A_N + D_N$) pathway will proceed through the top left corner of the plot, and a dissociative ($D_N + A_N$) pathway will proceed through the bottom left corner of the plot. Contrary to assumptions made by some authors (*1, 14, 53*), a concerted (A_ND_N) pathway need not proceed directly through the center of the plot but rather can

[1] Abbreviations: LFER, linear free energy relationship; PCM, polarized continuum model; MFJ, More O'Ferral Jencks; QM/MM, quantum mechanics/molecular mechanics; SCF, self-consistent field; PCM, polarized continuum model; QH, quasi-harmonic; RR, restraint release.

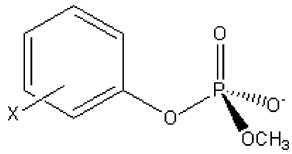

FIGURE 2: Prototype for the series of substituted methyl phenyl phosphate diesters examined in this work (*14*).

proceed through any part of the plot, depending on the nature of (i.e., whether it is associative or dissociative) and degree of asynchronicity in the transition state. Examining the system in this way is particularly valuable as it accounts for multiple mechanistic possibilities on the same free energy surface, as well as providing clear insight into the energetics of potential reaction pathways.

This work focuses on the analysis of the energetics and mechanism of attack of hydroxide on a series of homologous substituted methyl phenyl phosphate diesters in solution (Figure 2). On the basis of the experimental data, it has been assumed that the hydrolysis proceeds through a single concerted transition state (*14, 54, 55*) [similar to that calculated for the hydrolysis of *p*-nitrophenyl phosphate (*56*), though this transition state is dissociative], which has been assumed to be synchronous on the basis of LFER data (*14*). However, such an assumption is unjustified as the LFER cannot distinguish between a synchronous and (even slightly) asynchronous transition state.

There are already several theoretical gas-phase studies of the mechanism of phosphate diester hydrolysis, many of which are reviewed in ref *57*. However, these gas-phase studies often yield enormous reaction barriers of >80 kcal/mol, at which point the significance of a difference between a minimum of a few kilocalories per mole and its absence becomes questionable. Also, solution barriers for phosphate diester hydrolysis tend to be significantly lower. For instance, in the case of dimethyl phosphate hydrolysis, the activation Gibbs energy in the gas phase is computed to be 96 kcal/mol compared to the experimental value of 32 kcal/mol in solution (*58*). Finally, it is questionable if such gas-phase simulations of phosphate diester hydrolysis actually have any relevance to solving biological problems, since enzymatic reactions tend to take place in solution, and therefore, the solution reaction is the natural reference reaction to use for calibration for further QM/MM studies. Our aim is to explore the nature of the transition state without using an *a priori* assumption that the experimental information necessarily provides a unique clarification of this issue. Instead, we focus on reproducing available experimental data by computational approaches and then using the calculated free energy surfaces to explore the nature of the reaction coordinate and the transition state.

Computational studies involving hydroxide as a nucleophile are challenging, as this reaction has quite high activation entropies compared to systems where the nucleophile is water, for which the activation entropy is smaller by several kilocalories per mole (*59*). Standard *ab initio* packages cannot be used to accurately calculate the entropic contributions to reactions in solution, as they assume a harmonic potential for a very shallow reaction surface, thus overestimating the activation entropy (*60–62*). In this study, we evaluate configurational entropies using an empirical valence bond (EVB) surface (*50, 63*) with a bonding pattern corresponding to either the reactants or the transition states for phosphate diester hydrolysis. By combining a quasi-harmonic approximation with a restraint release approach as developed in refs *64* and *65* and refined in ref *66*, we are able to correctly evaluate the solute contribution to the overall activation entropy. It is important to bear in mind that our transition states are not simple gas-phase transition states but are rather obtained from full (i.e., unconstrained) optimizations in solution using the polarized continuum model (*67–70*). The initial structures for our transition state optimizations were obtained from careful examination of the free energy surface for the reaction and then subsequently characterized by further reaction coordinate mapping (see the Supporting Information). We reproduce ΔG_{exp} to within 1.3 kcal/mol for each compound studied and demonstrate that the hydrolysis mechanism for this series of phosphate esters is highly sensitive to the nature of the leaving group, preferring a compact A_ND_N mechanism at high pK_a values and a more expansive A_ND_N mechanism at lower pK_a values.

Overall, we believe that the characterization and quantification of the surface for the hydrolysis of phosphodiesters in solution are crucial for quantitative progress in QM/MM studies of enzyme catalysis of such systems, including studies of DNA polymerase in which different approaches lead to different conclusions (*35–41*).

THEORETICAL BASIS

The *ab initio* free energy surface for the hydrolysis of the parent compound was defined as a function of the distance from the phosphorus oxygen to the nucleophile (P−OH) and leaving group (P−OPh). For each point on the potential energy surface, these two distances were constrained, while all other degrees of freedom were allowed to freely optimize. It is important to bear in mind that this energy surface is actually a projection of the full free energy surface onto two dimensions. As a result, there are multiple points from the full free energy surface that correspond to each point on the MFJ plot, and any variation in coordinates not directly involved in bond making or bond breaking can add noise to the MFJ plot. At each point, the geometry and energy of the resulting structure have to be examined to verify that the true minimum energy for that point on the two-dimensional plot has been obtained. Therefore, it is very important that the MFJ plot is generated by careful reaction coordinate pushing, using a fine grid to minimize noise, which can otherwise obscure the location of key features on the free energy surface (*7, 10*).

All *ab initio* calculations were performed using Gaussian03 (*71*), and Becke's three-level hybrid functionals, which utilize a combination of Hartree–Fock exchange and density functional theory (DFT) exchange correlation (*72*). Initial gas-phase geometries were obtained using the 6-31+G* basis set, and the resulting structures were solvated using the COSMO continuum model (*73, 74*) and the 6-311+G** basis set. $P-O_{lg}$ distances were mapped out from 1.7 to 2.7 Å in 0.15 Å increments, and $P-O_{nuc}$ distances were mapped out from 1.7 to 2.7 Å in 0.1 Å increments (see the Supporting Information).

The free energy surface was used to identify the approximate geometry of the transition state, the correct geometry of which was obtained by an unconstrained

geometry optimization in solution using direct inversion in the iterative subspace (GDIIS) (*77, 78*), B3LYP/6-31+G*, and the polarized continuum model (PCM) with integral equation formalism (*67–70, 79*) which allows the calculation of the analytical gradients of the solute−solvent surface. A single-point energy correction was performed on the PCM-minimized stationary points using B3LYP/6-311+G** and the COSMO continuum model (see the Supporting Information). The parent transition state was then used as a template to obtain all other transition states for the series.

While the GDIIS method is known to be very effective in interpolation within the quadratic region of a desired stationary point, a known problem with this approach is its tendency to converge to the nearest critical point, even if this point is of an order different from the desired one (*80*) (i.e., in this case, a minimum rather than a saddle point). Therefore, the correct characterization of the transition state is greatly important. It should be noted that simulating solvation by means of applying a correction to the SCF energy using a continuum model rather than by including explicit water molecules in the simulation has a disadvantage in that it ignores possible proton transfer between water molecules. However, the only reported study where the presence of explicit water molecules has been demonstrated to reduce the barrier to the hydrolysis reaction is presented in ref *75*, and all our previous work showed that the presence of additional explicit water molecules does not reduce the barrier. This is discussed in detail in ref *76*. Additionally, the inclusion of explicit solvent molecules will introduce additional degrees of freedom into the system, any variation in which will create noise in the free energy surface. More crucially, the extra water molecules will make transition state determination virtually impossible (i.e., determining the precise unconstrained geometry as opposed to the approximate geometry obtained from the MFJ plot), as the presence of nonbonding interactions brought about by the loosely bound species we have introduced into the system will create a large number of soft vibrations that seriously complicate accurate identification of the correct transition state (see also ref *7*). Nevertheless, this issue is important and can only really be verified by the addition of explicit water molecules to the system and also by examination of the corresponding configurational entropy. QM/MM studies addressing this issue are underway in our research group. However, for the purposes of this work, we have simulated solvation using a continuum model and have obtained surprisingly accurate results using this approach.

Searching for gas-phase transition states involves evaluating the TS vibrational frequencies. This is extremely challenging in condensed phases and has not been accomplished in a satisfactory way for solution reactions with a flat energy surface in the region surrounding the TS. Thus, we prefer to use an approach similar to that used in our previous studies (e.g., refs *10* and *50*). That is, the starting structure for the transition state optimization is obtained by zooming in on the TS region of the original MFJ plot. The obtained transition state is then used as a starting structure to create a new map of all points within 0.1 Å of the transition state, using a fine (0.05 Å) grid. Using this careful mapping, we verify that our obtained transition states are indeed saddle points that correspond to the transition state expected from an examination of the full MFJ plot.

For each compound, solution geometries for the phosphate diester and the nucleophile were obtained using PCM/B3LYP/6-31+G*. An energy correction using COSMO/B3LYP/6-311+G** was performed for all three structures (diester, nucleophile, and transition state), and a correction for basis set superimposition error (BSSE) was performed on the transition state using counterpoise (*81, 82*). Zero-point energies were obtained from the calculation of gas-phase vibrational energies using Gaussian03. The reaction barrier was calculated relative to the sum energies of the phosphate diester and nucleophile (at infinite separation).

A shortcoming of both the PCM and COSMO solvation models is that they do not account for the solute contribution to the overall activation entropy, and this therefore needs to be calculated explicitly. The use of gas-phase vibrational frequencies is known to overestimate the solute activation entropy. Furthermore, the solute vibrations obtained from COSMO are known to be inaccurate (*60, 61*). Also, the harmonic approximation is particularly problematic when it comes to the crucial large amplitude reacting motions (*83–85*). One may try to use MD simulations of the solute motions, from which effective "quasi-harmonic" force constants can be computed (*86–91*). These force constants can then be used to compute thermodynamic properties such as entropy. However, careful studies have shown while the QH approximation functions quite well for simple systems with single-energy wells, it markedly overestimates the configurational entropy for systems with multiple occupied energy wells, as it merges multiple narrow energy wells into one broad energy well (*92*).

The difficulties in obtaining the contribution of the solute to the overall activation entropy can be overcome by means of a restraint release (RR) approach, introduced by Warshel and co-workers in 2000 (*64*). The idea behind this approach is to impose strong positional constraints on the Cartesian coordinates of the solute atoms in both the reactant state (RS) and transition state (TS) and to then subsequently evaluate the free energies associated with releasing these restraints. This can be written as

$$-T(\Delta S^{\ddagger})_{\mathrm{conf}} = \min(\Delta G_{\mathrm{RR}}^{\mathrm{TS}}) - \min(\Delta G_{\mathrm{RR}}^{\mathrm{RS}}) + T\Delta S_{\mathrm{cage}}^{\mathrm{RS}} \quad (2)$$

All RR free energies contain a residual contribution from the enthalpy of the system. However, this contribution approaches zero for restraint coordinates that give the lowest RR energy (*64, 93*). Therefore, the enthalpic contribution to $-T\Delta S_{\mathrm{conf}}$ is minimized by identifying the restraint coordinates that minimized ΔG_{RR} in both transition and reactant states, denoted by the min functions in eq 2. $\Delta S_{\mathrm{cage}}^{\mathrm{RS}}$ is the entropy associated with applying a $K = 0.3$ kcal mol^{-1} Å^{-2} restraint on a pair of reacting atoms to bring the reactant fragment from a molar volume to the same solvent cage. This entropy term was evaluated rigorously and analytically as a function of a special restraint used to keep the fragment at a predefined contact distance (in this case 3.0 Å), as outlined in ref *64*.

The approach used for this work is similar to that of ref *66* and involves a practical improvement to the original RR approach outlined in ref *64*. An initial 30 ps molecular dynamics simulation was performed on the RS and TS, with snapshots taken every 5 ps. MD simulations 20 ps in length were performed on each snapshot (with coordinates collected every 0.01 ps) to calculate the QH entropy for each snapshot,

Scheme 2: Simplified Overview of Phenyl Methyl Diester Hydrolysis

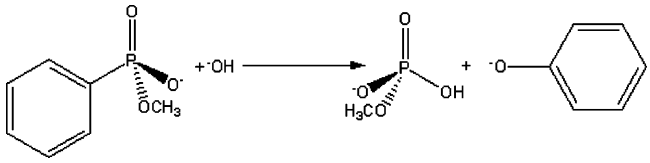

and this procedure was repeated for restraints 0, 0.3, 10, 20, and 30 kcal/mol in magnitude. This allows the calculation of the absolute entropy for these restraints. Subsequently, the free energy for the release of these restraints was evaluated using the RR approach. That is

$$-TS_{\text{conf}} = -TS(K = K_1)_{\text{QH}} + \min[\Delta G_{\text{RR}}(K = K_1 \rightarrow K = 0)] \quad (3)$$

where the subscript QH designates entropy computed by the quasi-harmonic approximation (*89*). It is important to emphasize that the solvent entropy is already included in the solvation free entropy (ΔG_{sol}) evaluated by implicit solvation models such as COSMO. What we evaluate here is the solute contribution to the overall activation entropy. All entropy calculations were performed using the Molaris software package, and the Enzymix force field (*94, 95*). Summing QM energies with activation entropies using a combined QH/RR approach allows us to accurately reproduce ΔG_{exp}.

RESULTS AND DISCUSSION

Parent System. The first reaction to be examined was the hydrolysis of the parent methyl phenyl diester (Scheme 2) (*14*). Figure 3a depicts the calculated surface for this system. From this figure, it can be seen that there is a single reaction pathway, corresponding to a concerted mechanism passing through an approximate transition state with P−O distances of 1.9 and 2.4 Å with respect to the leaving group and nucleophile, respectively, with no clear intermediate on the energy surface.

An unconstrained PCM geometry optimization of this structure yields an asymmetric concerted transition state, with actual P−O distances of 1.83 and 2.33 Å with respect to the leaving group and nucleophile, respectively (Figure 4). Figure 3b shows the surface obtained by high-resolution mapping around this transition state, verifying that it is indeed a maximum on the energy surface. After an energy correction had been performed using COSMO, the obtained barrier to this transition state relative to the moieties at infinite separation was 20.9 kcal/mol. The BSSE correction at the transition state was 3.3 kcal/mol, the zero-point energy 1.0 kcal/mol, and the calculated contribution of the solute to the overall activation entropy 4.8 kcal/mol, giving a total free energy of 30 kcal/mol which is in good agreement with the experimentally observed barrier of 28.6 kcal/mol.

Homologous Systems. We subsequently examined a series of homologous substituted methyl phenyl phosphate diesters, based on the LFER data provided by Herschlag and Zalatan (*14*). The compounds with the 4-nitro and 4-cyano phenyl substituents are known to be outliers from LFER for AP-catalyzed hydrolysis reactions (*9, 14, 96, 97*). However, we included these compounds in our study for the purpose of

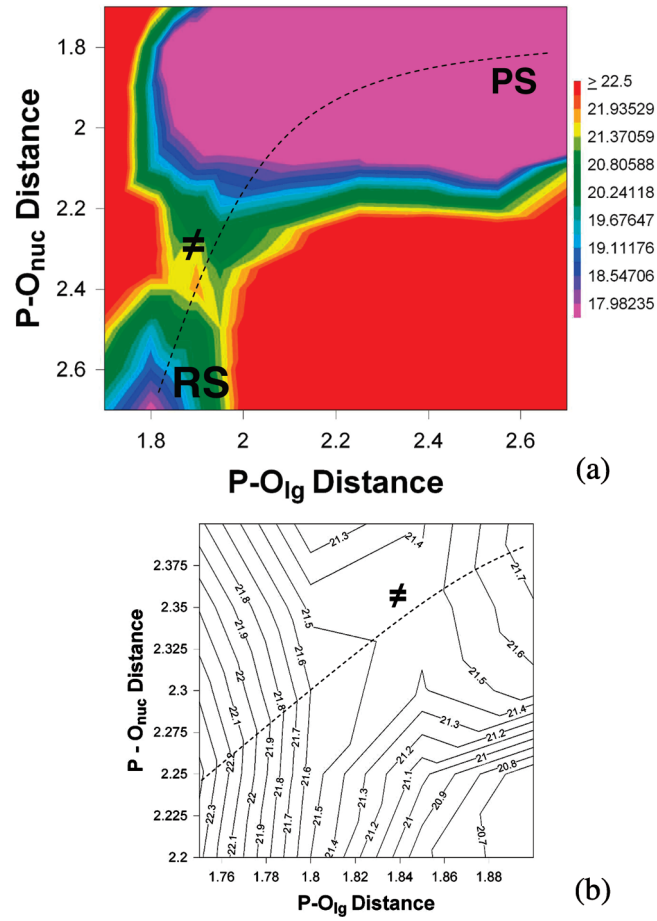

FIGURE 3: Calculated surfaces for (a) the hydrolysis of the unsubstituted methyl phenyl phosphate diester and (b) the region immediately surrounding the transition state obtained from surface a. All distances are in angstroms, and all relative energies are in kilocalories per mole.

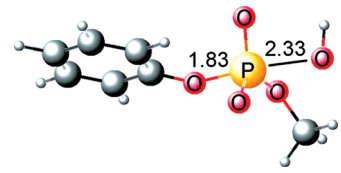

FIGURE 4: Transition state for methyl phenyl phosphate diester hydrolysis.

comparison. Table 1 shows the energy breakdown for each system. In each case, ΔG_{calc} was obtained by summing the change in the solute energy upon moving from the RS to the TS in the gas phase, the BSSE correction at the transition state, the solvation energy ($\Delta\Delta G_{\text{solv}}$), the solute polarization energy (ΔE_{pol}), the zero-point vibrational energy, and the contribution of the solute to the overall activation entropy, which is on average 4.7 kcal/mol (see the Supporting Information).

For comparison, cited values for the entropies of activation for representative monoanionic and dianionic S_N2 reactions in aqueous solution range from 5.7 to 9.2 kcal/mol (*19, 55, 98, 99*). Specifically, the experimental activation entropy for the 4-nitro compound is cited as 8.3 kcal/mol (*55*) as opposed to our calculated value of 4.2 kcal/mol. As emphasized in the methodology section, we are distinguishing between configurational and solvation entropy, and our value of 4.2 kcal/mol reflects the contribution (configurational) of the solute to the overall activation entropy. COSMO accounts

Table 1: Energy Decomposition for ΔG_{calc} (in kilocalories per mole)

substituent	pK_a	$\Delta E^{\circ}_{RS\rightarrow TS}$[a]	$\Delta\Delta G_{solv}$	ΔE_{pol}	ZPE	BSSE	$-T\Delta S$	ΔG_{calc}
4-nitro	7.14	74.2	−43.7	−14.4	0.7	3.4	4.2	24.4
4-chloro-3-nitro	7.78	75.3	−46.1	−12.6	0.8	3.5	4.1	25.0
4-cyano	7.95	78.1	−46.7	−14.0	1.0	3.5	4.5	26.4
3-nitro	8.35	71.6	−46.7	−6.7	0.6	3.5	5.0	27.3
3,4-dichloro	8.63	81.2	−50.0	−13.1	1.0	3.6	4.9	27.6
3-chloro	9.02	84.0	−52.4	−13.0	0.9	3.6	5.3	28.4
3-fluoro	9.28	85.6	−52.6	−13.8	1.0	3.6	4.6	28.4
4-chloro	9.38	84.7	−52.6	−13.0	1.0	3.6	4.8	28.5
4-fluoro	9.95	86.5	−52.7	−13.8	1.0	3.7	4.8	29.5
parent	9.95	69.8	−54.9	6.0	0.9	3.3	4.8	29.9

[a] $\Delta E^{\circ}_{RS\rightarrow TS}$ is the change in the solute energy upon moving from the RS to the TS.

Table 2: Correlation between the Experimental and Calculated Rate Constants and Activation Barriers[a]

substituent	pK_a	ΔG_{exp}	ΔG_{calc}	log k_{exp}	log k_{calc}
4-nitro	7.14	25.7	24.4	−5.2	−4.3
4-chloro-3-nitro	7.78	25.6	25.0	−5.1	−4.8
4-cyano	7.95	26.1	26.4	−5.5	−5.7
3-nitro	8.35	26.3	27.3	−5.6	−6.3
3,4-dichloro	8.63	27.0	27.6	−6.1	−6.4
3-chloro	9.02	27.5	28.4	−6.5	−7.3
3-fluoro	9.28	27.7	28.4	−6.6	−7.1
4-chloro	9.38	27.8	28.5	−6.7	−7.2
4-fluoro	9.95	28.4	29.5	−7.1	−7.9
parent	9.95	28.6	29.9	−7.2	−8.1

[a] All values are relative to the observed pK_a values for each compound studied. All energies are in kilocalories per mole.

for the solvation entropy, and the entropic contribution of the solvation model to the total free energy is not considered negligible (*99*). Therefore, this could account for the discrepancy between our calculated value and the experimental result. Table 2 shows the correlation among the rate constants, the activation barriers, and the observed pK_a values for each leaving group. Assuming an average value of 7.3 kcal/mol for the entropy on the basis of the values cited in the literature, which has been done by other groups (*19*), would overestimate the reaction barrier by up to 4 kcal/mol. Additionally, calculating accurate experimental values for activation entropies can be problematic, particularly if compensating entropy and enthalpy changes are involved in the reaction.

Also, while $\Delta\Delta G_{solv}$ increases with a decrease in pK_a, a similar trend is not seen in ΔE_{pol} (Table 1). For the parent compound, ΔE_{pol} is 6.0 kcal/mol. For the substituted compounds, ΔE_{pol} is on average –13.5 kcal/mol; that is, solute polarization decreases rather than increases the barrier. The exception to this is the 4-nitro compound for which the solute polarization energy is only –6.7 kcal/mol. Also, apart from the fact that the substituted compounds have a quite different value of ΔE_{pol} in comparison to the parent compound, there is no general trend in this value among the substituted compounds. Nevertheless, from Table 1, one can see that for each system, our value for ΔG_{calc} lies within 1.6 kcal/mol of ΔG_{exp}. It is interesting that in the case of the 4-nitro compound, which is a known outlier from the experimental LFER, k_{calc} actually matches the experimentally obtained LFER slightly better than k_{exp} does. The overall close correlation between observed and experimental LFERs for this series of compounds is demonstrated in Figure 5, emphasizing the importance of combining careful experimental and computational studies to obtain realistic free energies.

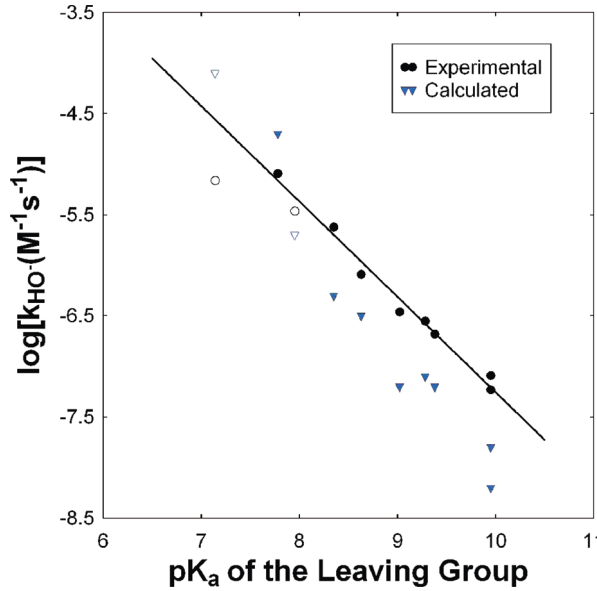

FIGURE 5: Experimental and calculated leaving group dependence for attack of hydroxide on methyl phenyl phosphate diesters. pK_a and log k_{OH} values are taken from Table 2. Experimental rate constants were measured at 42 °C (*14*).

Table 3: Changes in Phosphorus−Oxygen Distances with Respect to the Leaving Group and Nucleophile for Each Compound Examined

substituent	pK_a	P−O_{lg} distance (Å)	P−O_{nuc} distance (Å)
4-nitro	7.14	1.86	2.49
4-chloro-3-nitro	7.78	1.84	2.43
4-cyano	7.95	1.85	2.42
3-nitro	8.35	1.84	2.41
3,4-dichloro	8.63	1.84	2.40
3-chloro	9.02	1.84	2.38
3-fluoro	9.28	1.84	2.37
4-chloro	9.38	1.83	2.36
4-fluoro	9.95	1.83	2.35
parent	9.95	1.84	2.33

Of interest here is also the change in the P−O distances with respect to the leaving group and nucleophile in the transition state for each system (Table 3). In the parent system, the distances between the phosphorus atom and the leaving group and nucleophile oxygen atoms are 1.83 and 2.33 Å, respectively. There is little change in the P−O distance with respect to the leaving group (ranging from 1.83 to 1.86 Å). However, the change in the P−O distance with respect to the nucleophile is quite significant, moving steadily from 2.33 to 2.49 Å as the pK_a of the system is reduced, and this shift is more or less linearly proportional to the pK_a change. Again, this trend holds even for the structures that are expected to be outliers on the LFER.

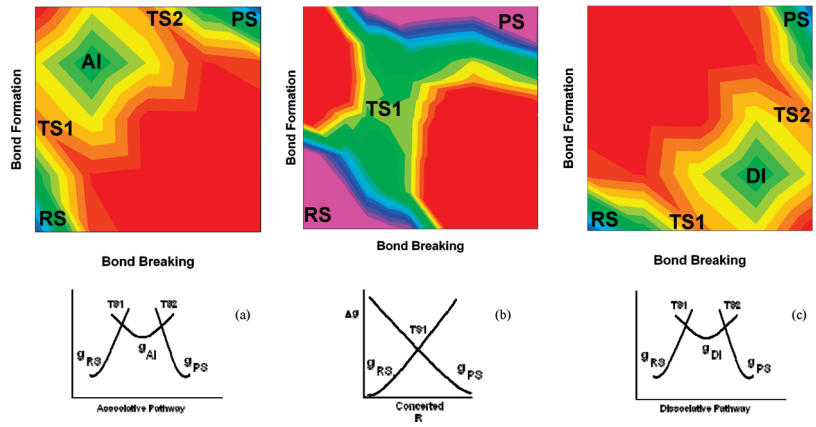

FIGURE 6: VB description of the energy surface for phosphate hydrolysis in the cases of (a) an associative, (b) a concerted, and (c) a dissociative mechanism. RS, PS, and TS represent reactant, transition, and product states, respectively. AI denotes an associative intermediate and DI a dissociative intermediate.

Implications for the Reaction Mechanism. We have performed a thorough analysis of the free energy surface for the parent compound and observe that the reaction preferentially proceeds through a single, concerted transition state. This trend is repeated for each subsequent compound studied. The experimental value of β_{lg} for this series of methyl phenyl phosphate diesters is cited as -0.94 ± 0.5 (*14*), and β_{eq} for substituted phenyl phosphate diesters is estimated to be -1.73 [where β_{eq} is the dependence of $\log(K_{eq})$ on the pK_a of the leaving group]. The β_{lg}/β_{eq} ratio is considered to represent the fractional effective charge in the transition state (*100, 101*). This quantity does not represent the actual partial charges, which have been demonstrated to be very similar for the associative and dissociative hydrolysis of phosphate monoester dianions (*10*). Nevertheless, this ratio can still be used as a rough guideline as to the type of reaction pathway one can expect from the LFER. For this series, β_{lg}/β_{eq} is equal to 0.5, suggesting a concerted transition state (*14*), with which our results are in good agreement. However, unlike the proposed synchronous transition states (*14*), we obtain asynchronous transition states, where the degree of asynchronicity is directly related to the pK_a of the leaving group.

Several studies which examine the ambiguity in the interpretation of the experimental LFER have been performed, demonstrating that different mechanistic possibilities for the same system can lead to similar LFERs (*10, 49, 50*). In essence, these studies describe the LFER by the empirical valance bond description (*10, 49, 50, 63*) in which the four corners of the free energy surface (Figure 1) are represented as centers of parabolic surfaces corresponding to different zero-order diabatic states (Figure 6). These parabolas can be mixed using the EVB off-diagonal term to generate the actual adiabatic reaction surface.

If the reaction follows one of the extreme reaction pathways (either associative or dissociative), the LFER can easily be quantified by shifting the parabolas in the bottom part of Figure 6 (*10, 49, 50, 63*). It has, however, been demonstrated that shifting the parabolas for different mechanistic possibilities can lead to similar LFERs (*10, 49, 50, 63*), suggesting the experimental LFERs do not have a unique mechanistic interpretation. This was most explicitly observed in a recent study by Klähn et al. (*10*), which accurately reproduced the LFER for a series of phosphate monoester dianions using computational studies and demonstrated that while hydrolysis is preferentially associative for leaving groups with high pK_a values, more acidic systems prefer a dissociative pathway, despite this not being observable in a mere examination of the experimental LFER. Once again, we observe a clear mechanistic shift from a compact transition state at high pK_a values to a more expansive transition state at low pK_a values, while accurately reproducing the experimental LFER for this series of substituted methyl phenyl diesters (Figure 5). Interpreting the LFER in the case of a concerted mechanism is particularly difficult, since unlike the situation with the stepwise pathways where there is a clear cutoff between associative and dissociative mechanisms, the transition between a compact and a more expansive concerted transition state can be quite smooth, as seen in Table 3, and easily missed when examining the experimental LFER.

Table 4: Metal−Metal Distances in Representative Metallophosphatase Crystal Structures from the Protein Data Bank (*7, 106*)

system	metal−metal distance (Å)
protein phosphatase 1 (1fjm)	3.27
purple acid phosphatase (1kbp)	3.32
inositol monophosphatase (1imd)	4.04
alkaline phosphatase (1alk)	4.12

Phosphatases that do not employ metal ions in catalysis generally have quite open active sites, making it easier to accommodate the expansive transition states and intermediates that would form in a dissociative pathway (*7*). In contrast to this, various reaction mechanisms proposed for metalloenzymes such as purple acid phosphatase, Ser/Thr phosphatases, inositol monophosphatase, and alkaline phosphatase involve an associative pathway (which can be either stepwise or concerted), and some, such as inositol monophosphatase, go so far as to completely engulf their substrates in the active site which would be inconsistent with a dissociative mechanism (*7, 97, 102–105*). Alkaline phosphatase (AP) stands out among these enzymes in that it can catalyze the hydrolysis of both phosphate mono- and diesters (*42, 43*). Table 4 shows metal−metal distances for representative metallophosphatase crystal structures from the Protein Data Bank (*7, 106*). From this table, it is seen that the longest metal−metal distance in the obtained crystal structures for these four enzymes is that of AP (4.12 Å). This is interesting when considering that there is a corresponding LFER for

the AP-catalyzed hydrolysis of the series of methyl phenyl diesters examined in this work (*14*). In the solution reactions, our most compact transition state is that of the parent compound with P−O distances of 1.83 and 2.33 Å with respect to the leaving group and nucleophile, respectively, corresponding to an associative A_ND_N pathway. The $P-O_{nuc}$ distance increases by up to 0.16 Å (to a P−O distance of 2.49 Å) with a decrease in pK_a. For an enzyme with a compact active site such as protein phosphatase 1 which has a metal−metal distance of 3.27 Å, such a large change in the size of the transition state would be highly significant and problematic. Of course, it is important to bear in mind that the metal sites in metalloenzymes are quite plastic, as well as the fact that the presence of metal ions in the active site could change the reaction mechanism (which was observed in the nonenzymatic system studied in ref *7*). However, on the basis of crystallographic data, the comparatively large AP active site could more easily allow for a mechanistic switch from a compact to an expansive transition state even in the enzyme-catalyzed reaction of metalloenzymes than say protein phosphatase 1, which has a much more compact active site. Nevertheless, it is important to perform careful QM/MM studies that check whether the solution-phase reaction is followed in the enzymatic system to verify this.

CONCLUSIONS AND FUTURE DIRECTIONS

Various detailed studies have demonstrated that the interpretation of experimental data for the hydrolysis of phosphate esters is at best ambiguous (*10, 49, 50*) and that experimental LFERs do not necessarily have unique mechanistic interpretations. Also, it is not possible to distinguish between a stepwise and a concerted pathway via examination of experimental LFERs. We have developed an improved computational protocol for studying phosphate monoester hydrolysis in solution, particularly when evaluating the contribution of the solute to the overall activation entropy, and have applied this protocol to the study of a series of homologous substituted methyl phenyl phosphate diesters. Of course, it could be suggested that our results need further validation by alternative computational approaches. We are in the process of improving the standard adiabatic charging (AC) free energy perturbation (FEP) procedure and will address this issue in a forthcoming work. However, the best validation is comparison to the experimental data, and we have demonstrated that we closely reproduce the experimental trend. In all cases, the reaction proceeds through a concerted A_ND_N mechanism which is compact at high pK_a values and becomes progressively more expansive in nature as the pK_a of the system is reduced. This observation is similar to the trend observed for phosphate monoester dianions in solution (*10*).

Studying enzyme-catalyzed reaction mechanisms still presents a major computational challenge. It is necessary not only to have a realistic reaction path obtained from correct sampling of the free energy surface, which can be done by careful QM/MM minimization, but also to evaluate the free energy changes associated with the reaction. This can be performed by a combined QM/MM and free energy perturbation (FEP) approach, where minimized structures along the enzymatic reaction coordinate are obtained by QM/MM minimization and the free energy associated with solvation of the reacting solute is obtained by FEP (see, for examples, refs *10* and *107*). To accurately model the interaction of the substrate with the surrounding system, it is necessary to use explicit solvent molecules and not a continuum solvation model. However, before the enzyme-catalyzed reaction is studied, it is important to have a clear understanding of the counterpart reaction in solution. Studying this by just QM/MM reaction coordinate following is problematic, as it requires an *a priori* assumption with regard to the nature of the reaction pathway. Here, we have examined the full free energy surface for methyl phenyl phosphate diester hydrolysis. The approach presented here is very versatile and can be applied to the study of any reaction which can be represented as a function of two reaction coordinates. Understanding the mechanism for the hydrolysis of phosphate diesters in solution opens doors for studying the mechanism of a range of phosphodiesterases, including alkaline phosphatase and more importantly DNA polymerases.

ACKNOWLEDGMENT

We thank Robert Rucker and Maciej Haranczyk for their assistance in the preparation of the manuscript.

SUPPORTING INFORMATION AVAILABLE

Validation of the solvation model. This material is available free of charge via the Internet at http://pubs.acs.org.

REFERENCES

1. Cleland, W. W., and Hengge, A. C. (2006) Enzymatic Mechanisms of Phosphate and Sulfate Transfer. *Chem. Rev. 106*, 3252–3278.
2. Benkovic, S. J., and Schray, K. J. (1973) *Chemical basis of biological phosphoryl transfer*, Academic Press, New York.
3. Vetter, I. R., and Wittinghofer, A. (1999) Nucleoside triphosphate-binding proteins: Different scaffolds to achieve phosphoryl transfer. *Q. Rev. Biophys. 32*, 1–56.
4. Westheimer, F. H. (1981) Monomeric metaphosphates. *Chem. Rev. 81*, 313–326.
5. Mildvan, A. S. (1979) The role of metals in enzyme-catalyzed substitutions at each of the phosphorous atoms of ATP. *Adv. Enzymol. Relat. Areas Mol. Biol. 49*, 103–126.
6. Cor, J. R., Jr., and Ramsey, O. B. (1964) Mechanisms of nucleophilic substitution in phosphate esters. *Chem. Rev. 64*, 317–352.
7. Kamerlin, S. C. L., and Wilkie, J. (2007) The role of metal ions in phosphate ester hydrolysis. *Org. Biomol. Chem. 5*, 2098–2108.
8. Gani, D., and Wilkie, J. (1995) Stereochemical, mechanistic and structural features of enzyme catalysed phosphate monoester hydrolysis. *Chem. Soc. Rev. 24*, 55–63.
9. Hollfelder, F., and Herschlag, D. (1995) The nature of the transition state for enzyme-catalyzed phosphoryl transfer. Hydrolysis of O-aryl phosphorothioates by alkaline phosphatase. *Biochemistry 34*, 12255–12264.
10. Klahn, M., Rosta, E., and Warshel, A. (2006) On the mechanism of hydrolysis of phosphate monoester dianions in solution and proteins. *J. Am. Chem. Soc. 128*, 15310–15323.
11. Florian, J., and Warshel, A. (1997) A fundamental assumption about OH- attack in phosphate hydrolysis is not fully justified. *J. Am. Chem. Soc. 119*, 4458–4472.
12. Florián, J., and Warshel, A. (1998) Phosphate ester hydrolysis in aqueous solution: Associative versus dissociative mechanisms. *J. Phys. Chem. B 102*, 719–734.
13. Wilkie, J., and Gani, D. (1996) Comparison of inline and non-inline associative and dissociative reaction pathways for model reactions of phosphate monoester hydrolysis. *J. Chem. Soc., Perkin Trans. 2 2*, 783–787.

14. Zalatan, J. G., and Herschlag, D. (2006) Alkaline phosphatases mono- and diesterase reactions: Comparative transition state analysis. *J. Am. Chem. Soc. 128*, 1293–1303.
15. Zalatan, J., Catrina, I., Mitchell, R., Grzyska, P., O'Brien, P., Herschlag, D., and Hengge, A. (2007) Kinetic Isotope Effects for Alkaline Phosphatase Reactions: Implications for the Role of Active-Site Metal Ions in Catalysis. *J. Am. Chem. Soc. 129*, 9789–9798.
16. Du, X., Black, G. E., Lecchi, P., Abramson, F., and Sprang, S. R. (2004) Kinetic isotope effects in Ras-catalysed GTP hydrolysis: Evidence for a loose transition state. *Proc. Natl. Acad. Sci. U.S.A. 101*, 8858–8863.
17. Sorensen-Stowell, K., and Hengge, A. C. (2005) Examination of P-OR bridging bond orders in phosphate monoesters using ^{18}O isotope shifts in ^{31}P NMR. *J. Org. Chem. 70*, 4805–4809.
18. Wolfenden, R., and Yuan, Y. (2006) Monoalkyl sulfates as alkylating agents in water, alkylsulfatase rate enhancements and the "energy rich" nature of sulfate half-esters. *Proc. Natl. Acad. Sci. U.S.A. 104*, 83–86.
19. Iché-Tarrat, N., Ruiz-Lopez, M., Barthelat, J.-C., and Vigroux, A. (2007) Theoretical evaluation of the substrate-assisted catalysis mechanism for the hydrolysis of phosphate monoester dianions. *Chem.—Eur. J. 13*, 3617–3629.
20. Feuerstein, J., Goody, R. S., and Webb, M. R. (1989) The mechanism of guanosine nucleotide hydrolysis by p21 c-Ha-ras. The stereochemical course of the GTPase reaction. *J. Biol. Chem. 264*, 6188–6190.
21. Langen, R., Schweins, T., and Warshel, A. (1992) On the mechanism of guanosine triphosphate hydrolysis in ras p21 proteins. *Biochemistry 31*, 8691–8696.
22. Schweins, T., Langen, R., and Warshel, A. (1994) Why have mutagenesis studies not located the general base in ras p21. *Nat. Struct. Biol. 1*, 476–484.
23. Chung, H.-H., Benson, D. R., and Schultz, P. G. (1993) Probing the structure and mechanism of RAS protein with an expanded genetic code. *Science 259*, 806–809.
24. Schweins, T., Geyer, M., Scheffzek, K., Warshel, A., Kalbitzer, H. R., and Wittinghofer, A. (1995) Substrate-assisted catalysis as a mechanism for GTP hydrolysis of p21ras and other GTP-binding proteins. *Nat. Struct. Biol. 2*, 36–44.
25. Shurki, A., and Warshel, A. (2004) Why does the Ras Switch "Break" By Oncogenic Mutations? *Proteins 55*, 1–10.
26. Glennon, T. M., Villa, J., and Warshel, A. (2000) How does GAP catalyze the GTPase reaction of Ras? A computer simulation study. *Biochemistry 39*, 9641–9651.
27. Schweins, T., Geyer, M., Kalbitzer, H. R., Wittinghofer, A., and Warshel, A. (1996) Linear free energy relationships in the intrinsic and GTPase activating protein-stimulated guanosine 5′-triphosphate hydrolysis of p21ras. *Biochemistry 35*, 14225–14231.
28. Admiraal, S. J., and Herschlag, D. (1995) Mapping the transition state for ATP hydrolysis: Implications for enzymatic catalysis. *Chem. Biol. 2*, 729–739.
29. Admiraal, S. J., and Herschlag, D. (2000) The substrate-assisted general base catalysis model for phosphate monoester hydrolysis: Evaluation using reactivity comparisons. *J. Am. Chem. Soc. 122*, 2145–2148.
30. Maegley, K. A., Admiraal, S. J., and Herschlag, D. (1996) Ras-catalyzed hydrolysis of GTP: A new perspective from model studies. *Proc. Natl. Acad. Sci. U.S.A. 93*, 8160–8166.
31. Schweins, T., and Warshel, A. (1996) Mechanistic analysis of the observed linear free energy relationships in p21ras and related systems. *Biochemistry 35*, 14232–14243.
32. Schweins, T., Geyer, M., Scheffzek, K., Warshel, A., Kalbitzer, H. R., and Wittinghofer, A. (1995) Substrate-assisted catalysis as a mechanism for GTP hydrolysis of p21ras and other GTP-binding proteins. *Nat. Struct. Biol. 2*, 36–44.
33. Grigorenko, B., Nemukhin, A. V., Cachau, R. E., Topol, I. A., and Burt, S. K. (2005) Computational study of a transition state analog of phosphoryl transfer in the Ras-RasGAP complex: AlF_x versus MgF. *J. Mol. Model. 11*, 503–508.
34. Hübscher, U., Maga, G., and Spadari, S. (2002) Eukaryotic DNA polymerases. *Annu. Rev. Biochem. 71*, 133–163.
35. Florian, J., Goodman, M. F., and Warshel, A. (2003) Computer Simulation of the Chemical Catalysis of DNA Polymerases: Discriminating between Alternative Nucleotide Insertion Mechanisms for T7 DNA Polymerase. *J. Am. Chem. Soc. 125*, 8163–8177.
36. Florián, J., Goodman, M. F., and Warshel, A. (2005) Computer Simulations of Protein Functions: Searching for the Molecular Origin of the Replication Fidelity of DNA Polymerases. *Proc. Natl. Acad. Sci. U.S.A. 102*, 6819–6824.
37. Xiang, Y., Oelschlager, P., Florián, J., Goodman, M. F., and Warshel, A. (2006) Simulating the Effect of DNA Polymerase Mutations on Transition State Energetics and Fidelity: Evaluating Amino Acid Group Contributions and Allosteric Coupling for Ionized Reisudes in Human Pol β. *Biochemistry 45*, 7036–7048.
38. Arndt, J. W., Gong, W., Xuejon, Z., Showalter, A. K., Liu, J., Dunlap, C. A., Lin, Z., Paxson, C., Tsai, M.-D., and Chan, M. K. (2001) Insight into the Catalytic Mechanism of DNA Polymerase β: Structures of Intermediate Complexes. *Biochemistry 40*, 5368–5375.
39. Lin, P., Pedersen, L. C., Batra, V. K., Beard, W. A., Wilson, S. H., and Pedersen, L. G. (2006) Energy Analysis of Chemistry for correct insertion by DNA polymerase β. *Proc. Natl. Acad. Sci. U.S.A. 103*, 13294–13299.
40. Wang, L., Yu, X., Hu, P., Broyde, S., and Zhang, Y. (2007) A Water-Mediated and Substrate-Assisted Catalytic Mechanism for *Sulfolobus solfataricus* and DNA Polymerase IV. *J. Am. Chem. Soc. 129*, 4731–4737.
41. Petellier, H., Sawaya, M. R., Kumar, A., Wilson, S. H., and Kraut, J. (1994) Structures of Ternary Complexes of Rat DNA Polymerase β, a DNA Template-Primer and ddCTP. *Science 264*, 1891–1903.
42. Coleman, J. E. (1992) Structure and Mechanism of Alkaline Phosphatase. *Annu. Rev. Biophys. Biomol. Struct. 21*, 441–483.
43. O'Brien, P. J., and Herschlag, D. (2001) Functional interrelationships in the alkaline phosphatase superfamily: Phosphodiesterase activity of *E. coli* alkaline phosphatase. *Biochemistry 40*, 5691–5699.
44. Galperin, M. Y., Bairoch, A., and Koonin, E. V. (1998) A superfamily of metalloenzymes unifies phosphopentomutase and cofactor-independent phosphoglycerate mutase with alkaline phosphatases and sulfatases. *Protein Sci. 7*, 1829–1835.
45. Galperin, M. Y., and Jedrzejas, M. J. (2001) Conserved core structure and active site residues in alkaline phosphatase superfamily enzymes. *Proteins 45*, 318–324.
46. Gijsberg, R., Ceulemans, H., Stalmans, W., and Bollen, M. (2001) Structural and catalytic similarities between nucleotide pyrophosphatases/phosphodiesterases and alkaline phosphatases. *J. Biol. Chem. 276*, 1361–1368.
47. Williams, A. (1992) *Adv. Phys. Org. Chem. 27*, 1–55.
48. Jencks, W. P. (1969) *Catalysis in chemistry and enzymology*, McGraw-Hill, New York.
49. Aqvist, J., Kolmodin, K., Florian, J., and Warshel, A. (1999) Mechanistic alternatives in phosphate monoester hydrolysis: What conclusions can be drawn from available experimental data? *Chem. Biol. 6*, R71–R80.
50. Florian, J., Aqvist, J., and Warshel, A. (1998) On the reactivity of phosphate monoester dianions in aqueous solution: Bronsted linear free-energy relationships do not have a unique mechanistic interpretation. *J. Am. Chem. Soc. 120*, 11524–11525.
51. Jencks, W. P. (1985) A primer for the bema hapothle. An empirical approach to the characterization of changing transition-state structures. *Chem. Rev. 85*, 511–527.
52. More O'Ferrall, R. A. (1970) Relationships between E2 and E1cB mechanisms of β-elimination. *J. Chem. Soc. B,* 274–277.
53. Ba-Saif, S. A., Davis, A. M., and Williams, A. J. (1989) Effective charge distrtibution for attack of phenoxide ion on aryl methyl phosphate monoanion: Studies related to the action of ribonuclease. *J. Org. Chem. 54*, 5483–5486.
54. Herschlag, D., and Jencks, W. (1989) Phosphoryl transfer to anionic oxygen nucleophiles. Nature of the transition state and electrostatic repulsion. *J. Am. Chem. Soc. 111*, 7587–7596.
55. Williams, N. H., Cheung, J., and Chin, J. (1998) Reactivity of phosphate diesters doubly coordinated to a dinuclear cobalt(III) complex: Dependence of the reactivity on the basicity of the leaving group. *J. Am. Chem. Soc. 120*, 8079–8087.
56. Zhang, L., Xie, D., Xu, D., and Guo, H. (2007) Supermolecule density functional calculations suggest a key role for solvent in alkaline hydrolysis of *p*-nitrophenyl phosphate. *Chem. Commun.,* 1638–1640.
57. Zhou, D.-M., and Taira, K. (1998) The hydrolysis of RNA: From theoretical calculations to the hammerhead ribozyme mediated cleavage of RNA. *Chem. Rev. 98*, 991–1026.
58. Dejaegere, A., Liang, X., and Karplus, M. (1994) Phosphate ester hydrolysis: Calculation of gas-phase reaction paths and solvation effects. *J. Chem. Soc., Faraday Trans. 90*, 1763–1770.

59. Schroeder, G. K., Lad, C., Wyman, P., Williams, N. H., and Wolfenden, R. (2006) The time required for water attack at the phosphorus atom of simple phosphodiesters and of DNA. *Proc. Natl. Acad. Sci. U.S.A. 103*, 4052–4055.
60. Florián, J., and Warshel, A. (1998) Phosphate ester hydrolysis in aqueous solution: Associative versus dissociative mechanisms. *J. Phys. Chem. B 102*, 719–734.
61. Philippe, Y. A., and Schlegel, H. B. (1998) Identification and treatment of internal rotation in normal mode vibrational analysis. *J. Chem. Phys. 108*, 2314–2325.
62. Iché-Tarrat, N., Barthelat, J.-C., Rinaldi, D., and Vigroux, A. (2005) Theoretical studies of the hydroxide-catalyzed P-O cleavage reactions of neutral phosphate triesters and diesters in aqeuous solution: Examination of the changes induced by H/Me substitution. *J. Phys. Chem. B 109*, 22570–22580.
63. Warshel, A. (1991) *Computer modeling of chemical reactions in enzymes and solutions*, John Wiley and Sons, New York.
64. Strajbl, M., Sham, Y. Y., Villa, J., Chu, Z. T., and Warshel, A. (2000) Calculation of activation entropies of chemical reactions in solution. *J. Phys. Chem. B 104*, 4578–4584.
65. Villa, J., Strajbl, M., Glennon, T. M., Sham, Y. Y., Chu, Z. T., and Warshel, A. (2000) How important are entropic contributions to enzyme catalysis? *Proc. Natl. Acad. Sci. U.S.A. 97*, 11899–11904.
66. Sharma, P. K., Xiang, Y., Kato, M., and Warshel, A. (2005) What are the roles of substrate assisted catalysis and proximity effects in peptide bond formation by the ribosome? *Biochemistry 44*, 11307–11314.
67. Cancès, M. T., Mennucci, B., and Tomasi, J. (1997) A new integral equation formalism for the polarizable continuum model: Theoretical background and applications to isotropic and anisotropic dielectrics. *J. Chem. Phys. 107*, 3032–3041.
68. Cossi, M., Scalmani, G., Rega, N., and Barone, V. (2002) New developments in the polarizable continuum model for quantum mechanical and classical calculations on molecules in solution. *J. Chem. Phys. 117*, 43–54.
69. Mennucci, B., and Tomasi, J. (1997) Continuum solvation models: A new approach to the problem of solute's charge distribution and cavity boundaries. *J. Chem. Phys. 106*, 5151–5158.
70. Tomasi, J., Mennucci, B., and Cancès, M. T. (1991) The IEF version of the PCM solvation method: An overview of a new method addressed to study molecular solutes at the QM ab initio level. *THEOCHEM 464*, 211–226.
71. Frisch, M. J, Trucks, G. W., Schlegel, H. B., Scuseria, G. E., Robb, M. A., Cheeseman, J. R., Montgomery, J. A., Jr., Vreven, T., Kudin, K. N., Burant, J. C., Millam, J. M., Iyengar, S. S., Tomasi, J., Barone, V., Mennucci, B., Cossi, M., Scalmani, G., Rega, N., Petersson, G. A., Nakatsuji, M., Hada, M., Ehara, K., Toyota, R., Fukuda, J., Hasegawa, M., Ishida, T., Nakajima, Y., Honda, Y., Kitao, O., Nakai, H., Klene, M., Li, X., Knox, J. E., Hratchian, H. P., Cross, J. B., Adacmo, C., Jaramillo, J., Gomperts, R., Stratmann, R. E., Yazyev, O., Austin, A. J., Cammi, R., Pomelli, C., Ochterski, J., Ayala, P. Y., Morokuma, K., Voth, G. A., Salvador, P., Dannenberg, J. J., Zakrzewski, V. G., Dapprich, S., Daniels, A. D., Strain, M. C., Farkas, Ö., Malick, D. K., Rabuck, A. D., Clifford, K., Cioslowki, J., Stefanov, B. B., Liu, G., Liashenko, A., Piskorz, P., Komaromi, I., Martin, R. L., Fox, D. J., Keith, T., Al-Laham, M. A., Peng, C. Y., Nanayakkara, A., Challacombe, M., Gill, P. M. W., Johnson, B. G., Chen, W., Wong, M. W., Gonzalez, C., and Pople, J. A. (2004)*Gaussian03*, revision C.02,Gaussian, Inc., Pittsburgh, PA.
72. Becke, A. D. (1993) Density-functional thermochemistry. III. The role of exact exchange. *J. Chem. Phys. 98*, 5648–5652.
73. Barone, V., and Cossi, M. (1998) Quantum calculation of molecular energies and energy gradients in solution by a conductor solvent model. *J. Phys. Chem. A 102*, 1995–2001.
74. Klamt, A., and Schüürmann, G. J. (1993) COSMO: A new approach to dielectric screening in solvents with explicit expressions for the screening energy and its gradient. *J. Chem. Soc., Perkin Trans. 2 5*, 799–805.
75. Hu, C.-H., and Brinck, T. (1999) Theoretical studies of the hydrolysis of the methyl phosphate anion. *J. Phys. Chem. A 103*, 5379–5386.
76. Glennon, T. M., Villa, J., and Warshel, A. (2000) How does GAP catalyse the GTPase reaction of Ras? A computer simulation study. *Biochemistry 39*, 9641–9651.
77. Csaszar, P., and Pulay, P. (1984) Geometry optimization by DIIS. *THEOCHEM 114*, 31–34.
78. Farkas, Ö., and Schlegel, H. B. (1999) Methods for optimizing large molecules. II. Quadratic search. *J. Chem. Phys. 111*, 10806–10814.
79. Mennucci, B., Cancès, M. T., and Tomasi, J. (1997) Evaluation of solvent effects in isotropic and anisotropic dielectrics and in ionic solutions with a unified integral equation method: Theoretical bases, computational implementation, and numerical applications. *J. Phys. Chem. B 101*, 10506–10517.
80. Farkas, Ö., and Schlegel, H. B. (2002) Methods for optimizing large molecules. *Phys. Chem. Chem. Phys. 4*, 11–15.
81. Simon, S., Duran, M., and Dannenberg, J. J. (1996) How does basis set superposition error change the potential surfaces for hydrogen-bonded dimers? *J. Chem. Phys. 105*, 11024–11031.
82. Boys, S. F., and Bernardi, F. (1970) The calculation of small molecular interactions by the differences of separate total energies. Some procedures with reduced errors. *Mol. Phys. 19*, 553–566.
83. Yildirim, T. (2002) Lattice Dynamics of Solid Cubane within the Quasiharmonic Approximation. *Solid State Commun. 124*, 449–455.
84. Della Valle, R. G., and Venuti, E. (1998) Quasiharmonic Lattice-Dynamics and Molecular Dynamics Calculations for the Lennard-Jones Solids. *Phys. Rev. B 58*, 206–212.
85. Allana, N. L., Barrerab, G. D., Purtonc, J. A., Simsa, C. E., and Taylora, M. B. (2000) Ionic solids at elevated temperatures and/or high pressures: Lattice dynamics, molecular dynamics, Monte Carlo and ab initio studies. *Phys. Chem. Chem. Phys. 2*, 1099–1111.
86. Levy, R., Rojas, O. L., and Friesner, R. A. (1984) Quasi-harmonic method for calculating vibrational spectra from classical simulations on multi-dimensional anharmonic potential surfaces. *J. Phys. Chem. 88*, 4233–4238.
87. Karplus, M., and Kuschick, J. N. (1981) Method for estimating the configurational entropy of macromolecules. *Macromolecules 14*, 325–332.
88. Rojas, O. L., Levy, R. M., and Szabo, A. (1986) Corrections to the quasiharmonic approximation for evaluating molecular entropies. *J. Chem. Phys. 85*, 1037–1043.
89. Levy, R., Karplus, M., Kuschisk, J., and Perahia, D. (1984) Evaluation of the configurational entropy for proteins: Application to molecular dynamics simulations of an α-helix. *Macromolecules 17*, 1370–1374.
90. Luo, H., and Sharp, K. (2002) On the calculation of absolute macromolecular binding free energies. *Proc. Natl. Acad. Sci. U.S.A. 99*, 10399–10404.
91. Swanson, J. M. J., Henchman, R. H., and McCammon, J. A. l. (2004) Revisiting free energy calculations: A theoretical connection to MM/PBSA and direct calculation of the association free energy. *Biophys. J. 86*, 67–74.
92. Change, C.-E., Chen, W., and Gilson, M. K. (2005) Evaluating the accuracy of the quasiharmonic approximation. *J. Chem. Theory Comput. 1*, 1017–1028.
93. Hermans, J., and Wang, L. (1997) Inclusion of Loss of Translational and Rotational Freedom in Theoretical Estimates of Free Energies of Binding. Application to a Complex of Benzene and Mutant T4 Lysozyme. *J. Am. Chem. Soc. 119*, 2707–2714.
94. Lee, F. S., Chu, Z. T., and Warshel, A. (1993) Microscopic and semimicroscopic calculations of electrostatic energies in proteins by the POLARIS and ENZYMIX Programs. *J. Comput. Chem. 14*, 161–185.
95. Sham, Y. Y., Chu, Z. T., Tao, H., and Warshel, A. (2000) Examining methods for calculations of electrostatic energies in proteins by the POLARIS and ENZYMIX Programs. *Proteins: Struct., Funct., Genet. 39*, 393–407.
96. Holtz, K. M., Cartrine, I. E., Hengge, A. C., and Kantrowitz, E. (2000) General acid-base catalysis of complex reactions in water. *Biochemistry 39*, 9451–9458.
97. Nikolic-Hughes, I., Rees, D. C., and Herschlag, D. (2004) Do electrostatic interactions with positively charged active site groups tighten the transition state for enzymatic phosphoryl transfer? *J. Am. Chem. Soc. 126*, 11814–11819.
98. Barnard, P. W. C., Bunton, C. A., Llewellyn, D. R., Vernon, C. A., and Welch, C. A. (1961) The reactions of organic phosphates. Part V. The hydrolysis of triphenyl and trimethyl phosphates. *J. Chem. Soc.,* 2670–2676.
99. Borden, J., Crans, D. C., and Florián, J. (2006) Transition state analogues for nucleotidyl transfer reactions: Structure and stability of pentavalent vanadate and phosphate ester dianions. *J. Phys. Chem. B 110*, 14988–14999.

100. Leffler, J. E. (1953) Parameters for the description of transition states. *Science 117*, 340–341.
101. Williams, A. (1984) Effective charge and Leffler's index as mechanistic tools for reactions in solution. *Acc. Chem. Res. 17*, 425–430.
102. Bone, R., Frank, L., Springer, J. P., Pollack, S. J., Osborne, S. A., Atack, J. R., Knowles, M. R., McAllister, G., Ragan, C. I., Broughton, H. B., Baker, R., and Fletcher, S. R. (1994) Structural analysis of inositol monophosphatase complexes with substrates. *Biochemistry 33*, 9460–9467.
103. Egloff, M.-P., Cohen, P. T. W., Reinemer, P., and Barford, D. (1995) Crystal structure of the catalytic subunit of human protein phosphatase 1 and its complex with tungstate. *J. Mol. Biol. 218*, 449–464.
104. Gani, D., and Wilkie, J. (1997) Metal ions in the mechanism of enzyme-catalysed enzyme phosphate monoester hydrolysis. *Struct. Bonding 89*, 133–175.
105. Kim, E. E., and Wyckoff, H. W. (1991) Reaction mechanism of alkaline phosphatase based on crystal structures. Two metal ion catalysis. *J. Mol. Biol. 218*, 449–464.
106. Berman, H. M., Westbrook, J., Feng, Z., Gilliland, G., Bhat, T. N., Weissig, H., Shindyalov, I. N., and Bourne, P. E. (2000) The protein data bank. *Nucleic Acids Res. 28*, 235–242.
107. Zhang, Y., Liu, H., and Yang, W. (2000) Free energy calculations on enzyme reactions with an efficient iterative procedure to determine minimum energy paths on a combined ab initio QM/MM potential energy surface. *J. Chem. Phys. 112*, 3483–3492.

BI702106M